Spectral properties of a one-dimensional extended Hubbard model from bosonization and time-dependent variational principle: Applications to one-dimensional cuprates

Hao-Xin Wang,[1,*] Yi-Ming Wu,[1,2,*] Yi-Fan Jiang,[3,†] and Hong Yao[1,‡]
[1]*Institute for Advanced Study, Tsinghua University, Beijing 100084, China*
[2]*Stanford Institute for Theoretical Physics, Stanford University, Stanford, California 94305, USA*
[3]*School of Physical Science and Technology, ShanghaiTech University, Shanghai 201210, China*

(Received 13 November 2022; revised 4 December 2023; accepted 11 December 2023; published 2 January 2024)

Motivated by recent angle-resolved photoemission spectroscopy (ARPES) experiments on doped one-dimensional (1D) cuprates, we investigate spectral properties of a 1D extended Hubbard model with both on-site repulsion U and nearest-neighbor interaction V, by employing bosonization analysis and the high-precision time-dependent variational principle (TDVP) calculations with large scale up to 300 sites. From state-of-the-art TDVP calculations, we find that the spectral weights of the holon-folding and $3k_F$ branches evolve oppositely as a function of V, and a moderate attractive V may best fit the experimental results, hinting at the possible existence of sizable electron-phonon coupling in cuprates. From bosonization analysis, we show that this peculiar dichotomy of holon-folding and $3k_F$ branches can be explained by a universal relation between the spectral intensity at arbitrary harmonic branches and the Luttinger parameters. We argue that the relation we establish can be used for detecting different interactions in various 1D systems.

DOI: 10.1103/PhysRevB.109.045102

I. INTRODUCTION

Understanding two- or three-dimensional strongly correlated systems has become one of the central challenges in condensed matter physics. For instance, there are still many open questions in cuprates including the mechanism of high-temperature superconductivity (SC), despite its being discovered for decades [1–6]. The reason why it's enormously hard to fully understand cuprates is twofold. On one hand, due to the lack of controllable analytical tools, it is almost impossible to exactly solve even simple models in two or higher dimensions. Although various numerical efforts including density matrix renormalization group (DMRG) [7–22] and determinant quantum Monte Carlo (QMC) methods [23–26] have been made to address the physical properties of the two-dimensional Hubbard model and closely related t-J models [27–29], reliably solving such two-dimensional (2D) strongly correlated problems is extremely challenging from theoretical side and is currently limited by the width of systems in DMRG [30] or by the notorious sign problem in QMC [31–37]. On the other hand, it is also difficult to know whether or not the model Hamiltonian in a theory under investigation has included all the necessary ingredients to capture the essential physics of a realistic system.

One way of avoiding these obstacles is to study one-dimensional (1D) systems, for which there exist many fruitful analytical tools and advanced numerical techniques such that microscopic models can be reliably solved and compared to experiments, if some 1D material is made available. Indeed, in a recent experimental breakthrough [38], the authors successfully synthesized 1D cuprates $Ba_{2-x}Sr_xCu\,O_{3+\delta}$ for various hole doping. An angle-resolved photoemission spectroscopy (ARPES) was then performed to investigate the spectral properties of, e.g., the spinon, holon, holon-folding (hf), and the $3k_F$ branches. Quite surprisingly, the observed spectral features, i.e., the spectral weight of $3k_F$ branch vanishes over a wide range of doping while that of hf branch remains visible all the time, are qualitatively different from those of the 1D Hubbard model, but can be best fitted using an extended Hubbard model with a nearest-neighbor (NN) attraction included (see Fig. 1 for details about the hf and $3k_F$ spectral branches). The NN attraction can be induced by nonlocal Holstein-like electron-phonon couplings (EPC), as shown in recent variational non-Gaussian exact diagonalization (NGSED) studies [39,40], and provides a hint about the potential importance of EPC in cuprates. However, it still remains unclear how an NN attraction can enhance the hf branch but suppress the $3k_F$ branch simultaneously. More generally, how the less singular $3k_F$ or even other higher harmonical branches are affected by microscopic interactions is not fully investigated.

In this paper, we employ both bosonization and time-dependent variational principle (TDVP) to study the 1D extended Hubbard model, with emphasis on understanding how the spectral peaks vary with NN interaction V as well as doping x. From large-scale TDVP calculations with up to 300 sites, we obtained the spectral function for various values of V and x. Our TDVP results showed that an attractive V can enhance the hf branch but suppress the $3k_F$ branch while a moderate repulsive V reverses the trend (Figs. 1 and 2), which are qualitatively consistent with [38–40]. This again hints at the presence of sizable EPC in cuprates. From bosonization, we establish a universal relation between the singular behavior of the spectral function at higher harmonical branches with the

*These authors contributed equally to the work.
†jiangyf2@shanghaitech.edu.cn
‡yaohong@tsinghua.edu.cn

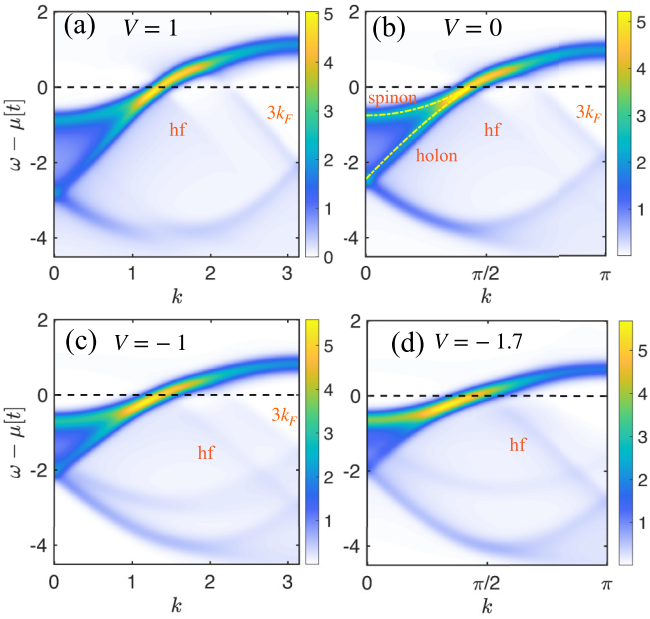

FIG. 1. Spectral functions calculated by TDVP for the extended Hubbard model [Eq. (1)] with doping $x = 14\%$ and $U = 8$ for various values of V between 1 and -1.7. For $V = 0$ in (b), the two yellow dashed lines depict the dispersions for spinon and holon. The holon folding (hf) and $3k_F$ branches are also marked. In (c) and (d), when the NN interaction V is tuned to the attractive side, we find that the $3k_F$ branch becomes more extinguished, in contrast to a sharper hf branch, which becomes more visible with sufficiently large $V = -1.7$.

Luttinger parameters determined by microscopic interactions. This relation explains the dichotomy of $3k_F$ spectral intensity between repulsive and attractive V, and can be used to detect different interactions for 1D systems by comparing the spectral functions.

II. SPECTRAL FUNCTION FROM TDVP

We begin with the Hamiltonian of 1D extended Hubbard model, which is given by

$$H = -t \sum_{\langle ij\rangle,\sigma} c^{\dagger}_{i\sigma} c_{j\sigma} + U \sum_{i} n_{i\uparrow} n_{i\downarrow} + V \sum_{\langle ij\rangle} n_i n_j, \qquad (1)$$

where $\langle ij\rangle$ denotes NN sites, $\sigma = \uparrow / \downarrow$, $n_{i\sigma} = c^{\dagger}_{i\sigma} c_{i\sigma}$, and $n_i = n_{i\uparrow} + n_{i\downarrow}$. In the 1D cuprate, $t \simeq 0.6$ eV and $U \simeq 8t$ [38,41]. Hereafter for simplicity we fix $U = 8t$ [42] and set $t = 1$ as the unit of energy. For electrons with Coulomb interactions, one naturally expects that the NN interaction V is repulsive. However, electron-phonon coupling (EPC) can generate an effective attractive NN interaction with retardation. Thus, we consider both cases of positive and negative V in our calculations. Thanks to the particle-hole symmetry of the extended Hubbard model, we only need to focus on the case of hole doping. The number of sites, electrons, and doping concentration are denoted by L, N, and $x = 1 - N/L$, respectively.

Over the past few years, much progress has been made in developing controllable numeric methods based on tensor-network states [43–47]. Among others, the time-dependent

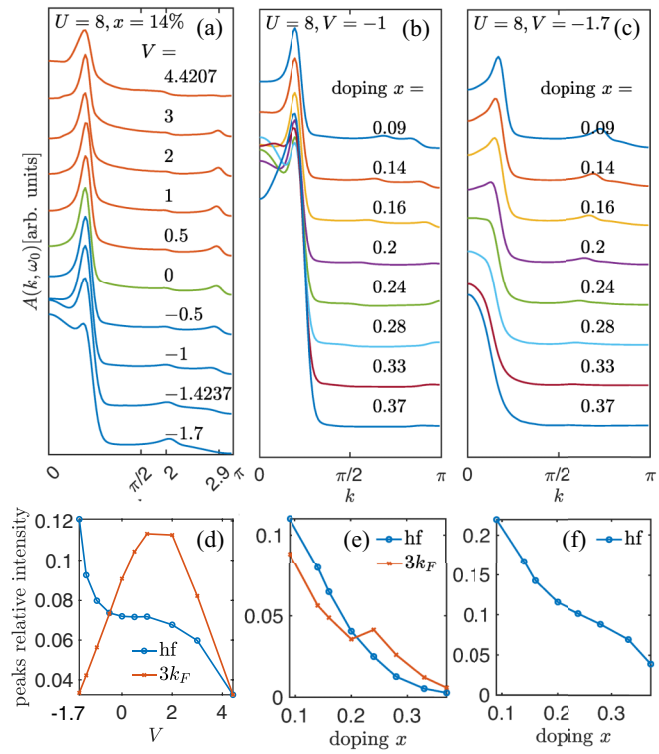

FIG. 2. Spectral functions of the $U = 8$. (a) MDCs under different V with doping concentration $x = 0.14$. The energy cuts ω_0 for different V range from -0.7 to -2.5 to match the major peak momenta. (b) MDCs of $V = -1$ at different doping x. The energy cuts are taken from -0.4 to -1.1 for the same reason in (a). (c) MDCs of $V = -1.7$ at different doping x. (d) hf and $3k_F$ peak intensities relative to the major peak as a function of V. The peak intensities are extracted from (a). (e), (f) hf and $3k_F$ peak relative intensities as a function of x. The peak intensities are extracted from (b) and (c), respectively.

variational principle (TDVP) is currently a state-of-the-art approach to calculate dynamic correlations in one dimension, thus being widely used to compute the spectral function in strongly correlated 1D systems [48–59]. The basic idea of TDVP is to project the time evolution of the wave function to the tangent space of the matrix product state (MPS) submanifold and offers the optimal way of the truncation step. According to the entanglement structure in 1D correlated systems, the MPS methods are generally more reliable than perturbation methods; the leading error of the first comes from the truncation error, which can be overcome by increasing bond dimensions. Here we implement the finite-size TDVP algorithm to calculate the retarded Green's function of electrons $G^R(x, t)$ and then obtain the spectral function $A(k, \omega)$ by performing a double Fourier transform. We analyze the finite-size effect to ensure the robustness of our numerics and the details can be found in the Supplementary Material (SM).

In Fig. 2 we show the calculated $A(k, \omega)$ from TDVP for the extended Hubbard model with various V and doping concentration x on system size $L = 100$. Figure 2(a) shows the momentum distribution curves (MDCs), i.e., $A(k, \omega)$ at some specific $\omega = \omega_0$, of the extended Hubbard model with different V (we plot $V > 0$ and $V < 0$ cases in different colors). For the pure Hubbard model with $V = 0$, the energy

cut is taken as $\omega_0 = -1.3$ measured from the Fermi energy. For the other values of V, we gradually shift ω_0 such that the hf and the $3k_F$ branches are most visible at momenta $k \simeq 2$ and $k \simeq 2.9$, respectively. The smallest value of $V = -1.7$ is close to the critical boundary and for $V \lesssim -1.8$ phase separation starts to appear in the ground state of the EHM.

It is clear from Fig. 2(a) that as V decreases from 1 to -1, the hf spectral weight stays almost intact; as V decreases further, the increases of hf become evident. Meanwhile, the $3k_F$ holon weight decreases monotonically. For $V > 1$, as V increases, the hf weight changes insignificantly, while the $3k_F$ weights suddenly drop at $V \approx V^* \equiv -U/[2\cos(2k_F)]$ (see SM for a detailed discussion). To clearly characterize the variation of these two weights, we extract the relative peak intensity, defined as the hf or $3k_F$ peak intensities divided by the major intensity, in Fig. 2(d). Here we do not use the Lorentzian peak fitting, but directly use the spectral weight. Both proper repulsive and attractive V can largely suppress $3k_F$ weight, but hf weight decays monotonically as V increases.

The dichotomous feature of k_F holon-folding and $3k_F$ holon spectral weight in the presence of V can be used to diagnose the interaction nature in 1D cuprates. In accord with the spectral behaviors reported in Ref. [38], the observed spectral weight of hf is fully evident, but that of the $3k_F$ branch disappears, which leads the authors to conclude that some NN attraction must exist in 1D BSCO material. Although both proper repulsive and attractive V can largely suppress $3k_F$ weight, repulsive $V \simeq 4.4$ is usually regarded as unrealistic in doped cuprates since the Coulomb repulsion is screened and becomes quite local. Our results show that at least for $U = 8t$, $V = -1.7$ yields the result consistent with the experiment's features.

We show the doping dependent MDCs with $U = 8$ at two different values of $V = -1$ and -1.7 in Figs. 2(b) and 2(c) and the corresponding peak relative intensities are shown in Figs. 2(e) and 2(f). The cases of $U = 8, V = -1$ at different doping were discussed in Ref. [38]. For $V = -1$ we find that the intensities of hf and $3k_F$ are comparable. However, for $V = -1.7$, the $3k_F$ intensity gets totally smeared out, and the hf weight decays more rapidly over increasing doping, which is consistent with the recent experimental results.

III. PHENOMENOLOGICAL BOSONIZATION

Bosonization is a powerful and reliable method for analyzing low-energy properties of 1D correlated models. In the low-energy limit, the linearized 1D dispersion allows for an exact identity relating the original fermion operators with bosonized field operators [60–63], and the interacting system of fermions may be turned into a free theory of bosons. However, in the higher-energy scale, the nonlinearity of the dispersion turns on interactions between bosons [64], which impedes our way of obtaining fermion properties by bringing about additional complexities in evaluating the expectation of boson field exponentials in an interacting bosonic theory.

Here we follow the seminal work by Haldane and adopt his phenomenological bosonization [65]. We start with the density operator, $\rho_s(x) = \sum_i \delta(x - x_i) = \sum_n |\nabla\phi_s(x)|\delta[\phi_s(x) - 2\pi n]$, where $\phi_s(x)$ is a monotonically increasing function of position, which takes the value $\phi_s(x_i) = 2\pi i$ at the position of the ith electron with spin polarization $s = \pm$. Here $\phi_s(x)$ is connected with the boson field $\Phi_s(x)$ by $\phi_s(x) = \pi\rho_0 x - \Phi_s(x)$ where ρ_0 is the average density of electrons per spin polarization and $\Phi_s(x) = [\Phi_\rho(x) + s\Phi_\sigma(x)]/\sqrt{2}$ with the subscripts ρ and σ labeling the charge and spin sector. Using the Poisson summation formula, the density operator can be rewritten as

$$\rho_s(x) = \left[\rho_0 - \frac{1}{\pi}\nabla\Phi_s(x)\right]\sum_{m\in\mathbb{Z}} \exp\{2im[\pi\rho_0 x - \Phi_s(x)]\}. \quad (2)$$

The fermion fields are followed by taking the square root of $\rho(x)$, and introducing another field $\Theta(x,t)$ to ensure the fermion anticommutation rule. Explicitly we have

$$\begin{aligned}\Psi_s(x,t) \sim \sum_{m\in\mathbb{Z}} \{&\exp(ic_m k_F x) \\ &\times \exp[-i\Theta_\rho(x,t)/\sqrt{2}] \times \exp[ic_m\Phi_\rho(x,t)/\sqrt{2}] \\ &\times \exp[-is\Theta_\sigma(x,t)/\sqrt{2}] \times \exp[isc_m\Phi_\sigma(x,t)/\sqrt{2}]\},\end{aligned} \quad (3)$$

where k_F is the Fermi momentum, $c_m = 2m + 1$ with m an integer. The leading harmonics is given by $c_m = \pm 1$, representing the right and left movers at $\pm k_F$, respectively. If only these two are kept, we arrive at the exact bosonization formula, for which the Hamiltonian is given by $H_0 = \frac{1}{L}\sum_{\nu,k}(\frac{\pi u_\nu K_\nu}{2}\Pi_\nu(k)\Pi_\nu(-k) + \frac{u_\nu}{2\pi K_\nu}k^2\Phi_\nu(k)\Phi_\nu(-k))$ with $\Pi_\nu(x) = \partial_x\Theta_\nu(x)/\pi$ [66]. Here K_ν is the Luttinger parameter and v_ν is the velocity for the ν-sector. Upon including higher harmonics, interacting terms between boson fields are effectively generated. However, we can assume that these interactions are weak, i.e., the nonlinearity of the original fermion dispersion is small as long as we are still in a low-energy scale. Then we can evaluate the single-particle Green's function using H_0. For instance, the retarded Green's function for the spin-up fermions is given by $G^R_\uparrow(x,t;x',t') \equiv -i\theta(t-t')\langle\{\Psi_\uparrow(x,t), \Psi^\dagger_\uparrow(x',t')\}\rangle_{H_0}$. A straightforward derivation shows that for the space-time translation invariant system $G^R_\uparrow(x,t;0,0) = \sum_m G^R_{\uparrow,(2m+1)k_F}(x,t)$, where

$$\begin{aligned}G^R_{\uparrow,(2m+1)k_F}(x,t) \sim -\theta(t)e^{ic_m k_F x}\mathrm{Re}\prod_{\nu=\rho,\sigma}\frac{1}{[\alpha + i(u_\nu t - x)]^{c_m/2}} \\ \times\left[\frac{\alpha^2}{(\alpha + iu_\nu t)^2 + x^2}\right]^{\gamma_{\nu,m}},\end{aligned} \quad (4)$$

where α is a cutoff with the scale of the lattice constant. The power index $\gamma_{\nu,m}$ is given by

$$\gamma_{\nu,m} = \frac{1}{8}\left(c_m^2 K_\nu + \frac{1}{K_\nu} - 2c_m\right), \quad (5)$$

where $K_{\nu=\sigma,\rho}$ are the Luttinger parameters that can be both estimated by either analytical g-ology [67] or more accurate numerical calculations (see below). For $m = 0$, the Green's function reduces to the well-documented results of the k_F branch [68–71], including the structure of spinon, holon, holon-folding, and antispinon, with different velocity $\pm u_{\rho/\sigma}$. The Green's function of the $3k_F$ branch also reproduces the earlier analysis [72] with $K_\rho = 1/2$. As an example, in

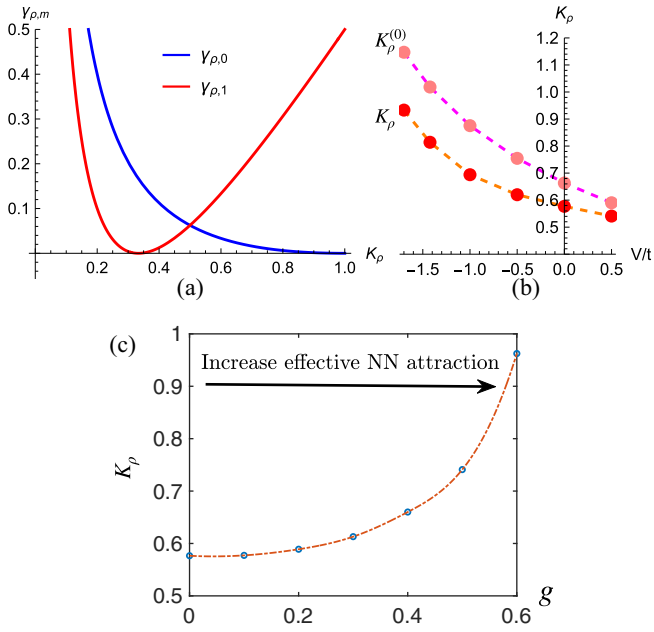

FIG. 3. (a) The exponent $\gamma_{\rho,m}$ as function of K_ρ. (b) K_ρ as a function of V, obtained from DMRG calculation, and the bare $K_\rho^{(0)}$ obtained from Eq. (8). (c)K_ρ as a function of EPC strength g in Hubbard-Holstein-like model, obtained from DMRG calculation. Model parameters: $U = 8t, \omega = 0.5t, g' = g/\sqrt{5}$, and doping concentration $x = 0.14$.

Fig. 3(a) we show $\gamma_{\rho,0}$ and $\gamma_{\rho,1}$ as a function of K_ρ. We see that $\gamma_{\rho,0}$ is a monotonically decaying function of K_ρ, while $\gamma_{\rho,1}$ is nonmonotonic, and at $K_\rho > 1/3$, $\gamma_{\rho,1}$ increases with K_ρ.

To obtain the spectral function $A(k, \omega)$, one needs to perform a 2D Fourier transformation on the retarded Green's function (4), which is, unfortunately, a rather involved task given the complexity of the function structure. Here, we focus on the singular behavior of $A(k, \omega)$ since they dominantly characterize the excitations. The spectral function of the k_F branch ($m = 0$) was studied in previous work [73–75]. A straightforward generalization to $m \neq 0$ leads to the singular spectral weight near the excitation dispersion

$$\begin{aligned} A_m(c_m k_F + q, \omega) \sim & |\omega - u_\rho q|^{2\gamma_{\sigma,m}+\gamma_{\rho,m}-1/2} \\ & \times |\omega - u_\sigma q|^{2\gamma_{\rho,m}+\gamma_{\sigma,m}-1/2} \\ & \times |\omega + u_\rho q|^{\gamma_{\rho,m}+2\gamma_{\sigma,m}}. \end{aligned} \tag{6}$$

The spectral functions here have either power-law divergence or cusp-singularity, similar to those at the k_F branch [66].

Now we apply Eq. (6) to the microscopic models. Since the model preserves the spin SU(2) symmetry, we have $K_\sigma = 1$ and hence $\gamma_{\sigma,m}$ remains constant. The only chance that V affects the spectral function is through K_ρ, or $\gamma_{\rho,m}$ equivalently. We then focus on the contributions related to $\gamma_{\rho,m}$. The hf and $3k_F$ branches are given by

$$\begin{aligned} \text{holon-folding:} \quad & A_0(k_F + q, \omega) \sim |\omega + u_\rho q|^{\gamma_{\rho,0}}, \\ 3k_F: \quad & A_1(3k_F + q, \omega) \sim |\omega - u_\rho q|^{\gamma_{\rho,1}}. \end{aligned} \tag{7}$$

To connect the above results with the microscopic interactions, we need to determine K_ρ from our extended Hubbard model. A simple calculation of K_ρ at the bare level in the weak-coupling limit gives

$$K_\rho^{(0)} = \sqrt{\frac{\pi v_F + V\cos(2k_F)}{\pi v_F + U + 4V - V\cos(2k_F)}}. \tag{8}$$

Going beyond the bare level, it acquires the renormalization from the sine-Gordon term $g_{\frac{1}{2n}}\cos[n\sqrt{8}\Phi_\rho(x)]$ at commensurate doping level p/n [67]. Here, we deploy the density matrix renormalization group (DMRG) calculation to extract renormalized K_ρ via the charge structure factor accurately. In a charge gapless phase, the charge structure factor has the form of $S_c(k) = K_\rho k/\pi$ [76]. We show the results in Fig. 3(b). It is clear that the renormalization effect only reduces the bare $K_\rho^{(0)}$, but does not change the overall trend as a function of V: as V goes from positive to negative, K_ρ increases. Consequently, $\gamma_{\rho,0}$ decreases while $\gamma_{\rho,1}$ increases, as shown in Fig. 3(a). According to Eq. (7), a typical weight of the hf or $3k_F$ branch scales as w^γ, with w being a small derivation from the excitation center ($\omega = \pm u_\rho q$) and a larger γ yields a smaller weight. It then explains why with some attractive V (and hence larger K_ρ) the $3k_F$ weight gets suppressed while the hf branch gets enhanced. This is consistent with our previous numeric observations.

Complementary to the extended-Hubbard model, we also studied a Hubbard-Holstein model which includes both onsite and NN EPC [39]

$$H_{\text{EPC}} = g\sum_i n_i(a_i^\dagger + a_i) + g'\sum_{\langle i,j\rangle} n_i(a_j^\dagger + a_j), \tag{9}$$

where $a_i^\dagger, a_i$ are phonon creation and annihilation operators. By fixing $U = 8t, \omega = 0.5t$, the doping level $x = 0.14$, and $g' = g/\sqrt{5}$, we show the DMRG calculated g-dependent Luttinger parameter K_ρ in Fig. 3(c). As g arises from 0 to 0.6, K_ρ increases to around 1, and according to our bosonization analysis above, will enhance the intensity of hf and suppress that of $3k_F$, which exhibits similar effects of NN attraction V. We note that further increasing g will drive the system into the phase separation.

IV. SUMMARY AND DISCUSSION

In this study, we investigated the spectral properties of the 1D extended Hubbard model, partly inspired by the recent ARPES experiment on the 1D cuprate BSCO [38] which shows a peculiar dichotomy between the holon-folding and the $3k_F$ spectra. We provide both analytical and accurate numerical evidence of how the holon-folding and $3k_F$ spectral weights vary with the NN density interaction V and doping x. Particularly, we found a relation between the spectral weight at higher harmonic branches and Luttinger parameters. When applied to 1D cuprates, this relation directly shows why introducing a sizable NN attraction is necessary to explain the experimental and numerical data, and also hints the noticeable presence of EPC in cuprates. We argue that it can also be applied in future studies on new 1D materials to establish microscopic models and analyze the nature of different interactions.

ACKNOWLEDGMENTS

We would like to thank Z.-X. Shen, T. Devereaux, H.-C. Jiang, and Z.-J. Wang for helpful discussions. This work is supported, in part, by the NSFC under Grant No. 11825404 (H.-X.W., Y.-M.W., and H.Y.), the MOSTC under Grant No. 2021YFA1400100 (H.Y.), the CAS Strategic Priority Research Program under Grant No. XDB28000000 (H.Y.), Shanghai Pujiang Program under Grant No. 21PJ1410300 (Y.-F.J.). Y.-M.W. was supported by the Shuimu Fellow Foundation at Tsinghua and also acknowledges the Gordon and Betty Moore Foundation's EPiQS Initiative through Grant No. GBMF8686 for support at Stanford.

APPENDIX A: NUMERIC CALCULATION OF SINGLE-PARTICLE SPECTRAL FUNCTION

We implement the finite-size TDVP to calculate the single-particle retarded Green's function, which is defined as

$$G^R_{\sigma\sigma'}(x,t;x',t') \equiv -i\theta(t-t')\langle\{c_\sigma(x,t), c^\dagger_{\sigma'}(x',t')\}\rangle, \quad \text{(A1)}$$

where $\{A,B\} = AB + BA$ is the anticommutator. After that, a double Fourier transform is applied to find the Green's function in momentum-frequency space $G^R_{\sigma,\sigma'}(k,\omega)$. The single-particle spectral function is followed by the imaginary part of the Green's function, namely,

$$A(k,\omega) = -\frac{1}{\pi}\sum_{\sigma,\sigma'} \mathrm{Im} G^R_{\sigma,\sigma'}(k,\omega). \quad \text{(A2)}$$

In practice, the TDVP code is imposed with the total particle number and total spin S_z conservation. When calculating the retarded Green's function, the Fermion operator at time slice $t = 0$ is fixed on the middle of the chain, by assuming the translation invariance [51]. The bond dimensions of MPS are retained $D = 500$–2000, which gives the truncation error magnitudes about 10^{-7}. We take open boundary conditions in accordance with the MPS' preference. The step size $\tau = 0.02$–0.03, and the maximum time $t_{\max} = 40$–90. The step error of such small τ can be neglected, and such a long time of correlation supports us to obtain the spectral functions brute-force, without any kind of extrapolation. In addition, when performing the Fourier transform $t \to \omega$, we multiply a Gaussian window $e^{-\alpha t^2}$ on the integral, with α's magnitude about 0.01. The aforestated parameters support a reliable dynamic simulation with high resolution.

As mentioned above, we assume the translation invariance and fix the Fermion operator at $t = 0$ in the middle of the chain, which significantly reduces the computational cost of simulations. However, the assumption only comes to be true in the thermodynamic limit $L \to \infty$. To plug up the loophole, we perform calculations of the spectral function on various system sizes and examine the finite-size scaling behavior. Figure 1(b) shows the momentum distribution curves (MDCs) at $\omega - \mu = -1$ of the Hubbard model, with parameters $U = 6$ and $x = 0.14$. The MDCs obtained from different sizes collapse onto each other, appearing indistinguishable to the naked eye. Based on this observation, we select a system size of $L = 100$ for the majority of calculations, treating the obtained data as representative of the thermodynamic limit.

We also carefully checked the convergence of the spectral functions obtained from simulation with different bond dimensions. In Fig. 4(c) we show the calculated spectral functions of the $L = 200$ system with two different bond dimensions $D = 500$ and 1000. The two curves of spectral functions from different bond dimensions almost overlap, indicating the negligible truncation error and the excellent convergence of our TDVP results.

APPENDIX B: PHENOMENOLOGICAL BOSONIZATION CALCULATION OF THE GREEN'S FUNCTION

There are various ways to obtain the single-particle correlation functions. A very convenient way is utilizing the boson coherent path integral. However, such an approach has to be supplemented by analytic continuation. Here we evaluate the correlation function directly in real-time space, and below are the explicit steps to obtain (4). The first step is to diagonalize the Hamiltonian $H_0 = \sum_\nu H_\nu$ using Bogoliubov transformation. After Fourier transformation into momentum space, we have

$$H_\nu = \frac{1}{L}\sum_k \left(\frac{\pi u_\nu K_\nu}{2}\Pi_\nu(k)\Pi_\nu(-k) + \frac{u_\nu k^2}{2\pi K_\nu}\Phi_\nu(k)\Phi_\nu(-k)\right). \quad \text{(B1)}$$

Introducing

$$\gamma_k = \frac{1}{\sqrt{2}}\left(\sqrt{\frac{|k|}{\pi K_\nu}}\Phi_\nu(k) + i\sqrt{\frac{\pi K_\nu}{|k|}}\Pi_\nu(k)\right),$$
$$\gamma^\dagger_k = \frac{1}{\sqrt{2}}\left(\sqrt{\frac{|k|}{\pi K_\nu}}\Phi_\nu(-k) - i\sqrt{\frac{\pi K_\nu}{|k|}}\Pi_\nu(-k)\right), \quad \text{(B2)}$$

it is easy to verify that these two operators obey $[\gamma_k, \gamma^\dagger_{k'}] = \delta_{k,k'}$. The inverse transformation is also easy to obtain

$$\Phi_\nu(k) = \sqrt{\frac{\pi K_\nu}{2|k|}}(\gamma_k + \gamma^\dagger_{-k}),$$
$$\Pi_\nu(k) = -i\sqrt{\frac{|k|}{2\pi K_\nu}}(\gamma_k - \gamma^\dagger_{-k}). \quad \text{(B3)}$$

Substitute Eq. (B3) to Eq. (B1), the diagonalized Hamiltonian is obtained

$$H_\nu = u_\nu \sum_k |k|\gamma^\dagger_k\gamma_k. \quad \text{(B4)}$$

Under this Hamiltonian, the time evolution of the free operator γ_k is simple, namely, $\gamma_k(t) = \gamma_k e^{-iu_\nu|k|t}$.

Next, we evaluate the Green's function using the diagonalized Hamiltonian (B4). Notice that the charge and spin sectors are decoupled, this fact enables us to write $G^>(x,t) = \langle\Psi^\dagger_{+,\uparrow}(x,t)\Psi_{+,\uparrow}(0,0)\rangle$ as a product of charge and spin contributions

$$G^>(x,t) = \prod_\nu \left\langle \exp\left(\frac{-i}{\sqrt{2}}[c_m\Phi_\nu(x,t) - \Theta_\nu(x,t)]\right) \times \exp\left(\frac{i}{\sqrt{2}}[c_m\Phi_\nu(0,0) - \Theta_\nu(0,0)]\right)\right\rangle_{H_\nu} \quad \text{(B5)}$$

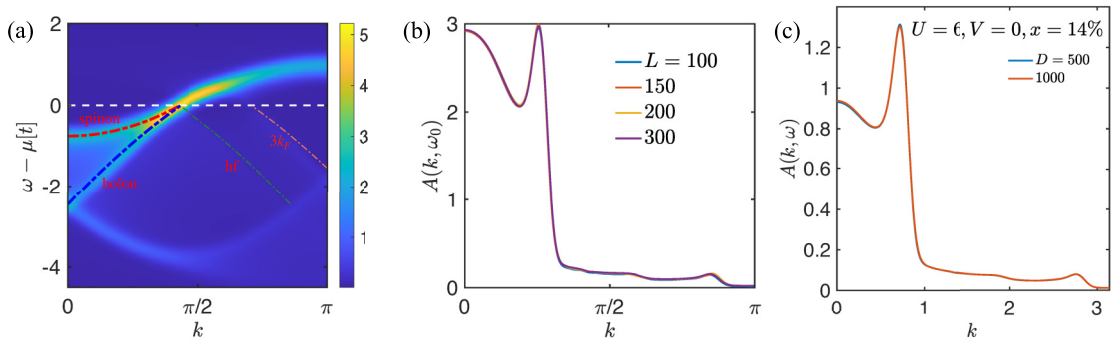

FIG. 4. (a) The colorscale plot of the spectral function of the Hubbard model at $U = 8$, length $L = 100$, and doping level $x = 0.14$. Only half of the Brillouin zone is drawn considering the parity symmetry. The white dashed line denotes the Fermi energy as a guide. The dash-dotted lines are the guides for the dispersion of low-energy excitations, including the spinon, holon, hf, and $3k_F$ branches. (b) The MDCs finite-size scaling of the Hubbard with $U = 6$ and doping $x = 0.14$, at energy cut $\omega - \mu = -1$. The curves of different sizes collapse well so that $L = 100$ is sufficiently large to represent the thermodynamic limit behavior. (c) The bond dimension convergence of the MDCs. The MDCs are calculated at $U = 6$, $x = 14\%$ Hubbard model on the $L = 200$ system. The energy cut is taken at $\omega - \mu = -7/6$. We see the MDCs calculated on $D = 500$ and 1000 collapse very well, which indicates the truncation errors in our calculation are negligible.

where the subscript H_v means average under H_v. For free boson Hamiltonians like Eq. (B1), the boson field is bilinear (Gaussian), and one can make use of the fact that the second-order cumulant expansion is exact, thus we evaluate the average using $\langle e^{iA}e^{-iB}\rangle = \exp(-\frac{1}{2}\langle A^2\rangle - \frac{1}{2}\langle B^2\rangle + \langle AB\rangle)$. For the charge contribution, we have

$$G^{>}_{\rho}(x,t) = \exp\left[\tfrac{1}{2}\langle[c_m\Phi_\rho(x,t) - \Theta_\rho(x,t)][c_m\Phi_\rho(0,0) - \Theta_\rho(0,0)]\rangle - \tfrac{1}{2}\langle[c_m\Phi_\rho(0,0) - \Theta_\rho(0,0)]^2\rangle\right]. \tag{B6}$$

In the exponential there are two parts, but we can skip the calculation of the second term since it can be obtained from the first term by taking the limit of $(x,t) \to (0,0)$. The operators in the first term, when written in momentum space are

$$\begin{aligned}
&\langle[c_m\Phi_\rho(x,t) - \Theta_\rho(x,t)][c_m\Phi_\rho(0,0) - \Theta_\rho(0,0)]\rangle \\
&= \frac{1}{L^2}\sum_{k,k'} e^{ikx}\left\langle\left(c_m\Phi_\rho(k,t) - \frac{\pi\Pi_\rho(k,t)}{ik}\right)\left(c_m\Phi_\rho(-k') + \frac{\pi\Pi_\rho(-k')}{ik'}\right)\right\rangle \\
&= \frac{\pi}{L^2}\sum_{k,k'} e^{ikx}\left\langle\left[c_m\sqrt{\frac{K_\rho}{2|k|}}(\gamma_k + \gamma^\dagger_{-k}) + \sqrt{\frac{|k|}{2K_\rho}}\frac{1}{k}(\gamma_k - \gamma^\dagger_{-k})\right]\left[c_m\sqrt{\frac{K_\rho}{2|k'|}}(\gamma_{-k'} + \gamma^\dagger_{k'}) - \sqrt{\frac{|k'|}{2K_\rho}}\frac{1}{k'}(\gamma_{-k'} - \gamma^\dagger_{k'})\right]\right\rangle \\
&= \frac{1}{2}\int_0^\infty dk\frac{e^{ikx}}{2k}\left(c_m^2K_\rho + \frac{1}{K_\rho} + 2c_m\right)e^{-iv_c|k|t} + \frac{1}{2}\int_0^\infty dk\frac{e^{-ikx}}{2k}\left(c_m^2K_\rho + \frac{1}{K_\rho} - 2c_m\right)e^{-iv_c|k|t}.
\end{aligned} \tag{B7}$$

To obtain the last line, we used the fact that at $T = 0$, the Bose distribution function $\langle\gamma^\dagger_k\gamma_k\rangle$ vanishes. The remaining integrals over k run from 0 to ∞. As we put in the main text that there exists an energy cutoff beyond which the bosonization procedure fails, thus for consistency the upper limit of the momentum integral cannot be taken formally as ∞. The cutoff is made by hand, and this can be done by introducing an exponentially decaying factor $e^{-\alpha k}$ into the integrand and the small parameter α has the same order of lattice constant. Collecting the results in Eq. (B7), the exponential in Eq. (B6) becomes

$$\begin{aligned}
&-\frac{1}{4}\left[\left(c_m^2K_v + \frac{1}{K_v}\right)\int_0^\infty dk\cdot e^{-\alpha k}\frac{1-\cos(kx)e^{-iu_v|k|t}}{k} - i2c_m\int_0^\infty dk\cdot e^{-\alpha k}\frac{\sin(kx)}{k}e^{-iu_v|k|t}\right] \\
&= \frac{1}{8}\left[\left(c_m^2K_v + \frac{1}{K_v}\right)\ln\frac{\alpha^2}{(\alpha + iu_vt)^2 + x^2} - 2c_m\ln\frac{\alpha + i(u_vt - x)}{\alpha + i(u_vt + x)}\right],
\end{aligned} \tag{B8}$$

which, in combination with $G^{<}(x,t)$, immediately gives Eq. (4).

APPENDIX C: MICROSCOPIC ORIGIN OF $3k_F$ BRANCH

We see from above that the $3k_F$ spectral weight can also be suppressed with a large repulsive V. Below we show that this peculiar behavior is closely related to the origin of the $3k_F$ branch. To address this issue, we note that the low-energy excitation modes are closely related to a singular behavior in the charge density distribution $n_k = \sum_{s=\uparrow,\downarrow} c^\dagger_{k,s}c_{k,s}$. For example, the holon/spinon excitation around k_F gives rise to a dip of n_k at the Fermi momentum k_F. Similarly, the $3k_F$ mode contributes to a hump structure in n_k at $k = 2\pi - 3k_F$. In Fig. 5(a), the blue curve shows these behaviors of n_k obtained by performing DMRG calculations for the Hubbard model with $U = 8$ and $V = 0$ at doping $x = 14\%$. Note that the singularity behaviors of n_k are directly connected to the spectral function via an integral.

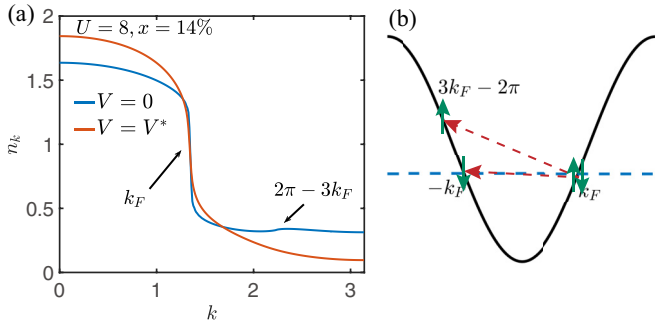

FIG. 5. (a) The charge density distribution n_k of EHM under two different $V = 0$ and $V = V^* \simeq 4.4207$. We choose $U = 8$ and doping level $x = 14\%$. The black arrows point to singularities associated with excitation modes emanating from different momenta. A hump around $k = 2\pi - 3k_F$ appearing at $V = 0$ corresponds to the $3k_F$ excitation. Under this special value of $V = V^*$, the singularity at $k = 2\pi - 3k_F$ disappears, implying the elimination of the $3k_F$ excitation. (b). The illustration of the umklapp $g_{3,\perp}$ process. The black curve is the dispersion and the blue dashed line is the Fermi energy. two right-moving particles (the green arrows) with opposite spin polarization around the Fermi surface are scattered to the left-moving side, one of which acquires momentum $k = 3k_F - 2\pi$.

It may be contrary to common sense why the particle number does not monotonically decrease as the band energy increases in the sense that the particles usually prefer lower energy states. The hump in high energy implies it may come from a gapped process, i.e., the umklapp scattering in the Hubbard model away from half-filling, which can be written as

$$H_3 = \int \mathrm{d}x \sum_{\sigma=\uparrow,\downarrow, s=L,R} g_{3,\perp} \Psi^\dagger_{s,\sigma} \Psi^\dagger_{s,-\sigma} \Psi_{-s,-\sigma} \Psi_{-s,\sigma}, \quad \text{(C1)}$$

where the argument x of the fermion field operators $\Psi_{s,\sigma}(x)$ is omitted for brevity. The process $g_{3,\perp}$ is schematically shown in Fig. 5(b). Obviously, the scattering transfers the particles around the Fermi surfaces to high-energy states with momentum $3k_F$, resulting in the singular hump in the particle number distribution n_k at $3k_F$. We numerically verified the above interpretation of origination of $3k_F$ in the EHM model, where $g_{3,\perp} = U + 2V\cos(2k_F)$. By increasing V to a critical value V^* which satisfies $U + 2V^*\cos(2k_F) = 0$, we expect that $g_{3,\perp}$ vanishes and hence the umklapp process is canceled, and as a result, the $3k_F$ mode disappears. We show n_k of the EHM model with $U = 8, V = V^*$ and $x = 14\%$ in Fig. 5(a). Clearly, the peak around $3k_F$ is smeared out, indicating the absence of $3k_F$.

APPENDIX D: DENSITY MATRIX RENORMALIZATION GROUP CALCULATION ON ELECTRON-PHONON COUPLING MODEL

We employ DMRG to extract the Luttinger parameter of the Hubbard-Holstein-like model in this work, whose Hamiltonian reads

$$\begin{aligned} H = &-t\sum_{i\sigma}(c^\dagger_{i\sigma}c_{i+1,\sigma} + \text{H.c.}) + U\sum_i n_{i,\uparrow}n_{i,\downarrow} \\ &+ g\sum_i n_i(a^\dagger_i + a_i) + g'\sum_{\langle i,j\rangle} n_i(a^\dagger_j + a_j) + \sum_i \omega a^\dagger_i a_i, \end{aligned} \quad \text{(D1)}$$

where the EPC terms are only taken up to the NN term g'.

Solving the above EPC models follows a standard DMRG procedure. However, incorporating the phonon modes, which are typically truncated to very large Hilbert space dimensions, results in computationally expensive calculations. To circumvent this issue, we employ the pseudosites scheme as proposed in Ref. [77]. The underlying concept involves truncating the Hilbert space dimension of the phonon mode to 2^M, subsequently decomposing a single phonon site into M pseudosites, each possessing a Hilbert space dimension of 2. We utilize a pseudosite count of $M = 5$ in our calculations, equivalent to phonon Hilbert space dimension 32. Under the parameters of $U = 8t, \omega = 0.5t, g' = g/\sqrt{5}$, and the strongest EPC case $g = 0.6t$, the occupancy number of the last pseudosite is about 6×10^{-5}, indicating the convergence with respect to the phonon Hilbert space dimension.

[1] B. Keimer, S. A. Kivelson, M. R. Norman, S. Uchida, and J. Zaanen, Nature (London) **518**, 179 (2015).
[2] E. Dagotto, Rev. Mod. Phys. **66**, 763 (1994).
[3] A. Damascelli, Z. Hussain, and Z.-X. Shen, Rev. Mod. Phys. **75**, 473 (2003).
[4] P. A. Lee, N. Nagaosa, and X.-G. Wen, Rev. Mod. Phys. **78**, 17 (2006).
[5] J. C. S. Davis and D.-H. Lee, Proc. Natl. Acad. Sci. USA **110**, 17623 (2013).
[6] E. Fradkin, S. A. Kivelson, and J. M. Tranquada, Rev. Mod. Phys. **87**, 457 (2015).
[7] S. R. White and D. J. Scalapino, Phys. Rev. Lett. **91**, 136403 (2003).
[8] C. Yang and A. E. Feiguin, Phys. Rev. B **93**, 081107(R) (2016).
[9] G. Ehlers, S. R. White, and R. M. Noack, Phys. Rev. B **95**, 125125 (2017).
[10] J. F. Dodaro, H.-C. Jiang, and S. A. Kivelson, Phys. Rev. B **95**, 155116 (2017).
[11] B.-X. Zheng, C.-M. Chung, P. Corboz, G. Ehlers, M.-P. Qin, R. M. Noack, H. Shi, S. R. White, S. Zhang, and G. K.-L. Chan, Science **358**, 1155 (2017).
[12] H.-C. Jiang, Z.-Y. Weng, and S. A. Kivelson, Phys. Rev. B **98**, 140505(R) (2018).
[13] H.-C. Jiang and T. P. Devereaux, Science **365**, 1424 (2019).
[14] Y.-F. Jiang, J. Zaanen, T. P. Devereaux, and H.-C. Jiang, Phys. Rev. Res. **2**, 033073 (2020).
[15] S. Gong, W. Zhu, and D. N. Sheng, Phys. Rev. Lett. **127**, 097003 (2021).
[16] H.-C. Jiang and S. A. Kivelson, Proc. Natl. Acad. Sci. USA **119**, e2109406119 (2022).
[17] Y. Gannot, Y.-F. Jiang, and S. A. Kivelson, Phys. Rev. B **102**, 115136 (2020).

[18] C.-M. Chung, M. Qin, S. Zhang, U. Schollwöck, and S. R. White (The Simons Collaboration on the Many-Electron Problem), Phys. Rev. B **102**, 041106(R) (2020).

[19] C. Peng, Y.-F. Jiang, Y. Wang, and H.-C. Jiang, New J. Phys. **23**, 123004 (2021).

[20] M. Qin, C.-M. Chung, H. Shi, E. Vitali, C. Hubig, U. Schollwöck, S. R. White, and S. Zhang (Simons Collaboration on the Many-Electron Problem), Phys. Rev. X **10**, 031016 (2020).

[21] S. Jiang, D. J. Scalapino, and S. R. White, Proc. Natl. Acad. Sci. USA **118**, e2109978118 (2021).

[22] M. Qin, T. Schäfer, S. Andergassen, P. Corboz, and E. Gull, Annu. Rev. Condens. Matter Phys. **13**, 275 (2022).

[23] S. R. White, D. J. Scalapino, R. L. Sugar, E. Y. Loh, J. E. Gubernatis, and R. T. Scalettar, Phys. Rev. B **40**, 506 (1989).

[24] J. P. F. LeBlanc, A. E. Antipov, F. Becca, I. W. Bulik, G. K.-L. Chan, C.-M. Chung, Y. Deng, M. Ferrero, T. M. Henderson, C. A. Jiménez-Hoyos *et al.* (Simons Collaboration on the Many-Electron Problem), Phys. Rev. X **5**, 041041 (2015).

[25] Z.-X. Li, F. Wang, H. Yao, and D.-H. Lee, Phys. Rev. B **95**, 214505 (2017).

[26] E. W. Huang, C. B. Mendl, H.-C. Jiang, B. Moritz, and T. P. Devereaux, npj Quantum Mater. **3**, 22 (2018).

[27] P. W. Anderson, Science **235**, 1196 (1987).

[28] F. C. Zhang and T. M. Rice, Phys. Rev. B **37**, 3759 (1988).

[29] D. P. Arovas, E. Berg, S. A. Kivelson, and S. Raghu, Annu. Rev. Condens. Matter Phys. **13**, 239 (2022).

[30] E. Stoudenmire and S. R. White, Annu. Rev. Condens. Matter Phys. **3**, 111 (2012).

[31] E. Y. Loh, J. E. Gubernatis, R. T. Scalettar, S. R. White, D. J. Scalapino, and R. L. Sugar, Phys. Rev. B **41**, 9301 (1990).

[32] M. Troyer and U.-J. Wiese, Phys. Rev. Lett. **94**, 170201 (2005).

[33] C. Wu and S.-C. Zhang, Phys. Rev. B **71**, 155115 (2005).

[34] Z.-X. Li, Y.-F. Jiang, and H. Yao, Phys. Rev. B **91**, 241117(R) (2015).

[35] Z.-X. Li, Y.-F. Jiang, and H. Yao, Phys. Rev. Lett. **117**, 267002 (2016).

[36] Z. C. Wei, C. Wu, Y. Li, S. Zhang, and T. Xiang, Phys. Rev. Lett. **116**, 250601 (2016).

[37] Z.-X. Li and H. Yao, Annu. Rev. Condens. Matter Phys. **10**, 337 (2019).

[38] Z. Chen, Y. Wang, S. N. Rebec, T. Jia, M. Hashimoto, D. Lu, B. Moritz, R. G. Moore, T. P. Devereaux, and Z.-X. Shen, Science **373**, 1235 (2021).

[39] Y. Wang, Z. Chen, T. Shi, B. Moritz, Z.-X. Shen, and T. P. Devereaux, Phys. Rev. Lett. **127**, 197003 (2021).

[40] Y. Wang, I. Esterlis, T. Shi, J. I. Cirac, and E. Demler, Phys. Rev. Res. **2**, 043258 (2020).

[41] M. S. Hybertsen, E. B. Stechel, M. Schluter, and D. R. Jennison, Phys. Rev. B **41**, 11068 (1990).

[42] We note that the onsite U used in this paper should be interpreted as the total onsite interaction combining both the original Hubbard onsite repulsion and the EPC-induced onsite attraction.

[43] R. Orús, Ann. Phys. (NY) **349**, 117 (2014).

[44] J. I. Cirac, D. Pérez-García, N. Schuch, and F. Verstraete, Rev. Mod. Phys. **93**, 045003 (2021).

[45] G. Evenbly, Front. Appl. Math. Stat. **8**, 806549 (2022).

[46] R. Orús, Nat. Rev. Phys. **1**, 538 (2019).

[47] F. Verstraete, V. Murg, and J. Cirac, Adv. Phys. **57**, 143 (2008).

[48] J. Haegeman, J. I. Cirac, T. J. Osborne, I. Pižorn, H. Verschelde, and F. Verstraete, Phys. Rev. Lett. **107**, 070601 (2011).

[49] J. Haegeman, T. J. Osborne, and F. Verstraete, Phys. Rev. B **88**, 075133 (2013).

[50] J. Haegeman, C. Lubich, I. Oseledets, B. Vandereycken, and F. Verstraete, Phys. Rev. B **94**, 165116 (2016).

[51] Y. Tian and S. R. White, Phys. Rev. B **103**, 125142 (2021).

[52] J.-W. Li, A. Gleis, and J. von Delft, arXiv:2208.10972.

[53] Y. Xu, Z. Xie, X. Xie, U. Schollwöck, and H. Ma, JACS Au **2**, 335 (2022).

[54] B. Kloss, Y. B. Lev, and D. Reichman, Phys. Rev. B **97**, 024307 (2018).

[55] Y. Wu, Phys. Rev. B **102**, 134306 (2020).

[56] M. Yang and S. R. White, Phys. Rev. B **102**, 094315 (2020).

[57] P. Secular, N. Gourianov, M. Lubasch, S. Dolgov, S. R. Clark, and D. Jaksch, Phys. Rev. B **101**, 235123 (2020).

[58] K. Hémery, F. Pollmann, and D. J. Luitz, Phys. Rev. B **100**, 104303 (2019).

[59] S. Paeckel, T. Köhler, A. Swoboda, S. R. Manmana, U. Schollwöck, and C. Hubig, Ann. Phys. (NY) **411**, 167998 (2019).

[60] S. Mandelstam, Phys. Rev. D **11**, 3026 (1975).

[61] R. Heidenreich, R. Seiler, and D. A. Uhlenbrock, J. Stat. Phys. **22**, 27 (1980).

[62] A. Luther and I. Peschel, Phys. Rev. B **9**, 2911 (1974).

[63] D. C. Mattis, J. Math. Phys. **15**, 609 (1974).

[64] F. D. M. Haldane, J. Phys. C **14**, 2585 (1981).

[65] F. D. M. Haldane, Phys. Rev. Lett. **47**, 1840 (1981).

[66] J. Voit, Rep. Prog. Phys. **58**, 977 (1995).

[67] T. Giamarchi, *Quatnum Physics in One Dimension* (Clarendon, Oxford, 2004).

[68] J. Sólyom, Adv. Phys. **28**, 201 (1979).

[69] J. Voit, Eur. Phys. J. B **5**, 505 (1998).

[70] Y. Suzumura, Prog. Theor. Phys. **63**, 51 (1980).

[71] H. J. Schulz, J. Phys. C **16**, 6769 (1983).

[72] Y. Ren and P. W. Anderson, Phys. Rev. B **48**, 16662 (1993).

[73] E. Orignac, M. Tsuchiizu, and Y. Suzumura, Phys. Rev. B **84**, 165128 (2011).

[74] V. Meden and K. Schönhammer, Phys. Rev. B **46**, 15753 (1992).

[75] J. Voit, J. Phys.: Condens. Matter **5**, 8305 (1993).

[76] D.-W. Qu, B.-B. Chen, H.-C. Jiang, Y. Wang, and W. Li, Commun. Phys. **5**, 257 (2022).

[77] E. Jeckelmann and S. R. White, Phys. Rev. B **57**, 6376 (1998).